Journal of
Marine Science and Engineering

MDPI

Article

Comparative Study of Air Resistance with and without a Superstructure on a Container Ship Using Numerical Simulation

Jun Seok [1] and Jong-Chun Park [2,*]

[1] Research Institute of Medium & Small Shipbuilding, Kangseo-gu, Busan 46757, Korea; jseok@rims.re.kr
[2] Department of Naval Architecture and Ocean Engineering, Pusan National University, Geumjeong-gu, Busan 46241, Korea
* Correspondence: jcpark@pnu.edu

Received: 16 March 2020; Accepted: 6 April 2020; Published: 9 April 2020

check for updates

Abstract: This study investigated the resistance performance of ships, using the air resistance correction method. In general, air resistance is calculated using an empirical formula rather than a direct calculation, as the effect of air resistance on the total resistance of ships is relatively smaller than that of water. However, for ships with large superstructures, such as container ships, LNG (liquefied natural gas) carriers, and car-ferries, the wind-induced effects might influence the air resistance acting on the superstructure, as well as cause attitude (trim and sinkage) changes of the ship. Therefore, this study performed numerical simulations to compare the total resistance, trim, and sinkage of an 8000 TEU-class container, ship with and without superstructures. The numerical simulation conditions were verified by comparing them with the study results of the KCS (KRISO Container Ship) hull form. In addition, the differences in the above values between the two cases were compared using the coefficients calculated by the empirical formula to identify the effects on the air resistance coefficient.

Keywords: air resistance; container ship; superstructure; numerical simulation; trim

---

1. Introduction

Shipyards and ship design engineering companies are continuously making numerous efforts to improve the performance of their ships, to satisfy the requirements of clients and meet various environmental regulations.

The performance of a ship is determined by various factors, such as speed, fuel oil consumption (FOC), and deadweight. In particular, speed is the major indicator of a ship's performance and is one of the performance aspects that are guaranteed, through a sea trial after construction.

Although there are various methods, including attaching an appendage to improve the ship's speed, the most basic method is to improve the resistance performance by optimizing the hull form of a ship. Therefore, shipyards and ship design engineering companies continue to invest heavily in improving the existing hull forms or developing new hull forms. In addition, various methods are used to reliably estimate the resistance performance of newly developed ships.

Traditionally, model test using a basin has been employed to estimate the resistance performance of ships. However, with the recent developments in computer technologies, numerical simulations using computational fluid dynamics (CFD) have attracted attention as a replacement for experimental methods.

In the beginning, analysis using numerical simulations was performed only on the sub-surface portion of the ship, without considering the free surface. Since then, the analysis methods have evolved to consider other aspects, such as the free surface and variation in the ship's attitude for accurate performance estimation. In addition, full-scale numerical simulation [1–3] of a ship, which is difficult to perform with the latest experimental methods, numerical simulation considering the hull roughness [4,5], and various other studies are underway.

In general, the estimation of resistance of a full-scale ship, through numerical simulations, is performed in the same method as in the experiment. First, a numerical simulation is performed for a model ship, which is a downsized model of a full-scale ship, and the total resistance value obtained from this simulation is used to estimate the resistance of the full-scale ship.

While estimating the resistance performance of a full-scale ship in the experimental method, as well as in the numerical simulation method, the air resistance acting on the superstructure, which has a relatively smaller effect on resistance performance than water, is estimated using an empirical formula without directly considering the superstructure [6].

However, for ships with large superstructures, such as container ships, LNG carriers, and car ferries, wind could not only affect the resistance acting on the superstructure but could also cause variation in the ship's attitude.

The variation in the ship's attitude is one of the factors that can directly affect the resistance performance [7–9]. As the resistance acting on the ship can increase or decrease according to the ship's attitude, an analysis that considers the superstructure is required for an accurate estimation of resistance performance.

Therefore, in this study, the effects of the presence or absence of the superstructure were evaluated by analyzing the resistance performance in two different cases; a model ship of an 8000 TEU-class container ship, with superstructures and without superstructures.

2. Model-Ship Correlation Method

2.1. Details of the 8000 TEU-Class Container Ship

The ship used for the analysis of resistance performance was an 8000 TEU-class container ship with 322.6-m L.B.P. (length between perpendiculars), 45.6-m breadth, and 24.6-m depth. The details are as provided in Table 1. The model ship for numerical simulations was set to 7.279 m, which was the same size as the KCS (3600 TEU KRISO Container ship).

In order to consider the superstructure, the ship was modeled with the containers loaded, as shown in Figure 1a, and the container was designed in a simple rectangular shape. In addition, breakwater, hatch cover, and accommodation were included in the modeling, whereas the lashing structures for the containers were omitted. Figure 1b shows a ship without superstructures, generally used for experiment in basin and numerical simulations.

Table 1. Principal dimensions of the 8000 TEU-class container ship (center of gravity means, from A.P. (Aft Perpendicular) to F.P. (Forward Perpendicular), centerline, from baseline to upward).

Item	Full Scale	Model Scale
Scale ratio	1:1	1/44.322
L.B.P (m)	322.6	7.279
Breadth (m)	45.6	1.029
Depth (m)	24.6	0.555
Draft (m)	13.0	0.293
Volume of displacement (m^3)	112,693.0	1.294
Wetted surface area (m^2)	16644.0	8.473
Center of gravity (m)	154.487, 0.0, 7.237	3.486, 0.0, 0.163
k_{xx}/Breadth	0.4	
k_{yy}/L.B.P, k_{zz}/L.B.P	0.25	

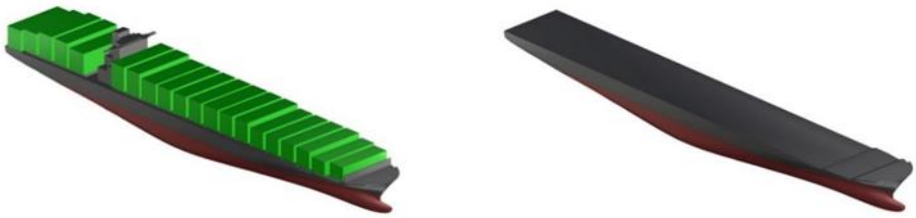

(a) **(b)**

Figure 1. Modeling of the 8000 TEU-class container ship. (**a**) Design of model with superstructure. (**b**) Design of model without superstructure.

2.2. Full-Scale Prediction Method

In the full-scale prediction method, the total resistance coefficient (C_{TS}) was calculated by a two-dimensional method, as the sum of the frictional resistance coefficient (C_F), residuary resistance coefficient (C_R), correlation allowance (C_A), and air resistance coefficient (C_{AA}), as shown in Equation (1). C_F is calculated according to the ITTC-1957 (International Towing Tank Conference-1957) frictional correlation line, C_A is calculated by the Harvald formulation, and C_{AA} is calculated by the ITTC method [6].

$$C_{TS} = C_F + C_R + C_A + C_{AA} \tag{1}$$

$$C_F = \frac{0.075}{(\log R_N - 2)^2} \tag{2}$$

$$C_R = C_{TM} - C_{FM} \tag{3}$$

$$C_A = \frac{0.5\log(\Delta) - 0.1(\log(\Delta))^2}{10^3} \tag{4}$$

$$C_{AA} = C_{DA}\frac{\rho_A \cdot A_{VS}}{\rho_S \cdot S_S} \tag{5}$$

where Δ is the displacement in ton, R_N is the Reynolds number, and C_{DA} is the air drag coefficient of the ship above the water line that can be determined through the wind tunnel testing or calculations. Typically, 0.8 can be used as the default value of C_{DA} in the range 0.5–1.0 if the specific value is not known [6]. ρ_A is the density of air, ρ_S is the density of seawater, A_{VS} is the projected area of the ship above the water line to the transverse plane, and S_S is the wetted surface area of the ship. The subscript M signifies the model and S signifies the full-scale ship.

3. Numerical Simulation

In this study, the commercial software Star-CCM+ was used to perform the numerical simulation. The governing equations were the continuity equation and momentum equation for three-dimensional unsteady incompressible viscous flow, shown in Equations (6) and (7) [10].

$$\frac{\partial U_i}{\partial x_i} = 0 \tag{6}$$

$$\frac{\partial U_i}{\partial t} + U_j\frac{\partial (U_i)}{\partial x_j} = -\frac{1}{\rho}\frac{\partial p}{\partial x_i} + \frac{1}{\rho}\frac{\partial}{\partial x_j}\left(\mu\frac{\partial U_i}{\partial x_j} - \rho\overline{u_i' u_j'}\right) + B \tag{7}$$

where U is the average velocity vector, x is the coordinate system, t is the time, ρ is the density, p is the pressure, and μ is the coefficient of viscosity. $\rho\overline{u_i' u_j'}$ is the turbulent shear stress that is determined using a turbulence model, and B is the body force. In this study, a realizable k-ϵ model was used for the turbulence model.

The governing equations mentioned above were discretized using the finite volume method (FVM). The convection and diffusion terms were discretized with the second-order upwind scheme. The second-order implicit scheme was used for temporal discretization.

The semi-implicit method for a pressure-linked equations (SIMPLE) algorithm was used for velocity-pressure coupling. The volume of fluid (VOF) method with a high-resolution interface capturing (HRIC) algorithm was used to define the water and air area of the free surface.

Equation (8) related to the translation of the center of mass of the body, and Equation (9) related to the rotation of the body, formulated with the origin at the center of mass of the body.

$$m\frac{dv}{dt} = f \tag{8}$$

$$M\frac{d\vec{\omega}}{dt} + \vec{\omega} \times M\vec{\omega} = \mathrm{n} \tag{9}$$

where m is the mass of the body, f is the force acting on the body, v is velocity of the center of mass, M is the tensor of the inertia moments, $\vec{\omega}$ is the angular velocity of the rigid body, and n is the moment acting on the body.

3.1. Initial Conditon and Boundary Condition

In the numerical simulation, the length, breadth, and height directions were set as 4.0 L, 1.5 L, and 2.5 L, as shown in Figure 2a. Here, L is the L.B.P. of the ship.

As shown in Figure 2b, velocity inlet, pressure outlet, symmetry, no-slip wall of the ship, and free-slip wall conditions were used for each boundary. To limit the calculation time, only half the breadth of the ship was modeled and the symmetry boundary condition was applied. Heave and pitch motion were considered by using the dynamic body fluid interaction (DFBI) method for the translation and rotation of the entire domain. The total calculation time of the numerical simulation was 90 s and the time increment was 0.02 s.

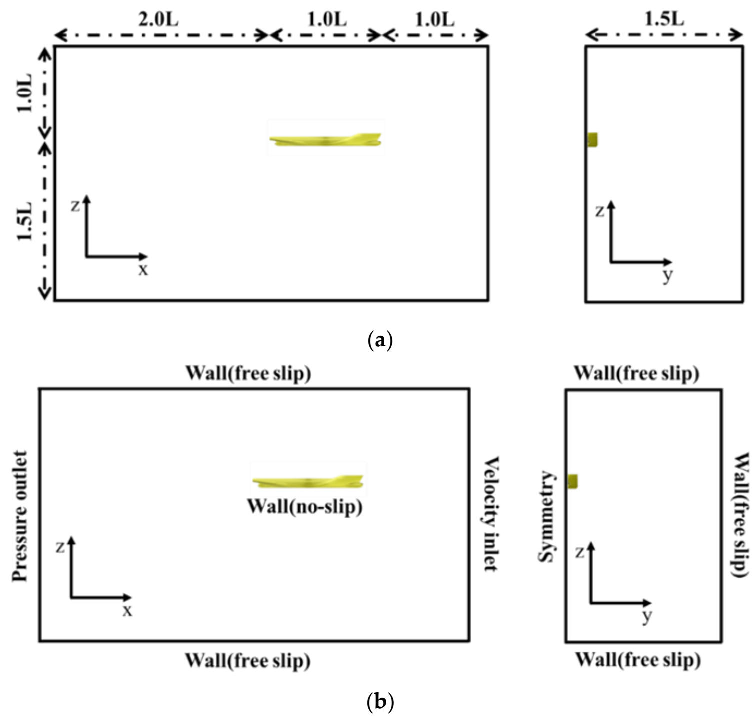

Figure 2. Computational domain and boundary conditions for numerical simulation; (**a**) computational domain and (**b**) boundary condition.

The above conditions were verified by conducting numerical simulations using the KCS hull form. KCS is a popular hull form like KVLCC (KRISO Very Large Crude-Oil Carrier) and DTMB (David Taylor Model Basin) it is often used to verify the conditions of numerical simulation through comparisons with experimental data [11–14]. Table 2 shows the main particulars of the KCS hull form; numerical simulation was performed for the model scale.

Table 2. Principal dimensions of KCS (center of gravity means (from A.P. to F.P., centerline, from baseline to upward)).

Item	Model Scale
Scale ratio	1/31.599
L.B.P (m)	7.279
Breadth (m)	1.019
Depth (m)	0.601
Draft (m)	0.342
Volume of displacement (m^3)	1.649
Wetted surface area (m^2)	9.544
Center of gravity (m)	3.532, 0.0, 0.230
k_{xx}/Breadth	0.4
k_{yy}/L.B.P, k_{zz}/L.B.P	0.25

3.2. Grid System

The grid system for the numerical simulation consisted of approximately 1.5 million cells, as shown in Figure 3. It was created using surface re-mesher, prism layer, and trimmer grid, which are auto-meshing methods provided by Star-CCM+. Five layers were generated in the normal direction to the hull, to consider the viscous flow field. In addition, we arranged the grid more closely around the free surface, to consider the wave generated by the hull. The minimum size of a cell was set to 1.0×10^{-2} m and Y^+ was less than 100 for the entire area of the hull, as shown in Figure 4. Additional numerical simulation was performed to validate the grid sensitivity of the 8000 TEU container ship, with the superstructure, as shown in Table 3.

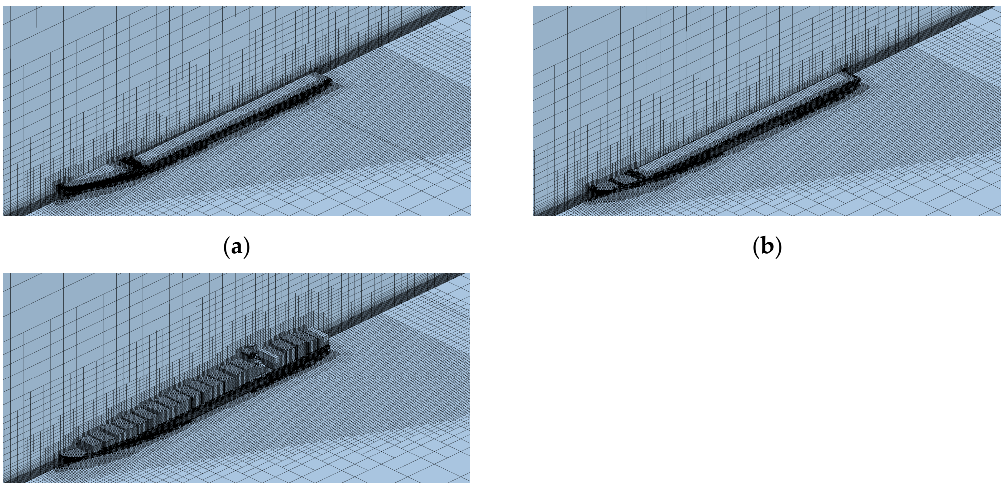

(a) (b) (c)

Figure 3. Grid system for numerical simulation. (**a**) KCS, (**b**) 8000 TEU-class container ship without superstructure, and (**c**) 8000 TEU-class container ship with superstructure.

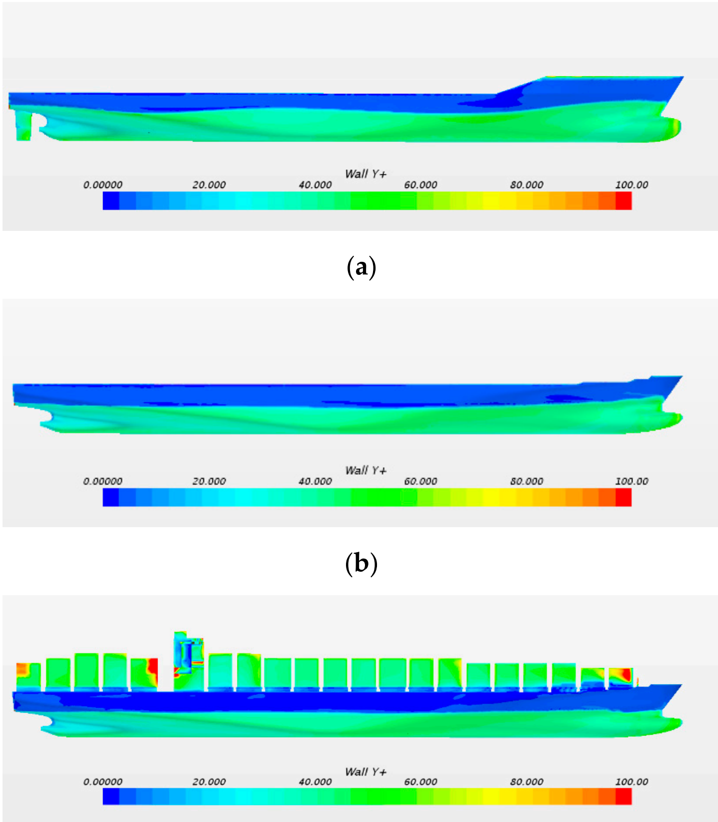

(**a**)

(**b**)

(**c**)

Figure 4. Y^+ entire area of the hull. (**a**) KCS, (**b**) 8000 TEU-class container ship without superstructure, and (**c**) 8000 TEU-class container ship with superstructure.

Table 3. Results of the grid dependency test of the 8000 TEU container ship, with superstructure.

F_N	$C_{TM} \times 10^3$		
	Coarse (Approx. 1.0 million)	**Medium (Approx. 1.5 million)**	**Fine (Approx. 2.0 million)**
0.274	3.823	3.771	3.750

As the number of grids increased from coarse to fine, C_{TM} tended to converge. In particular, since the difference in C_{TM} between the medium and the fine grid system was less than 1%, so the medium grid was applied to reduce the calculation time in numerical simulation.

4. Results of the Numerical Simulation

4.1. Validation Study

Numerical simulations were conducted under six different speed conditions (Froude number (F_N) of 0.108, 0.152, 0.195, 0.227, 0.260, 0.282) for validation of the simulation conditions. The results are as shown in Figure 5.

As shown in Figure 5a, the sinkage tended to increase as the speed increased. As shown in Figure 5b, the trim by stern tended to increase as speed increased, when F_N was at or below 0.269 and decreased when F_N exceeded 0.269. Overall, under the six speed conditions, the results for trim and sinkage were quantitatively similar to the experimental simulation results [11], when compared with the numerical simulation results of Villa et al. [14]. However, a quantitative difference from the experiment results was observed for the trim when F_N was less than 0.15 or more than 0.28, and for the sinkage when F_N was 0.16 or below. A difference of approximately 3% was observed from the experimental value of the total resistance coefficient, at the low speed of F_N = 0.108. Overall, the results were quantitatively similar to the experimental results under all the six speed conditions. It was also relatively more consistent with the experimental results than the numerical simulation results of Villa et al. [14], as shown in Figure 5c.

Therefore, as the accuracy of the numerical simulations for the ship's attitude appeared to be relatively low in the low-speed range (F_N < 0.16) or in the high-speed range (F_N > 0.28), the numerical simulations of the 8000 TEU-class container ship were conducted in the F_N range of 0.16–0.27.

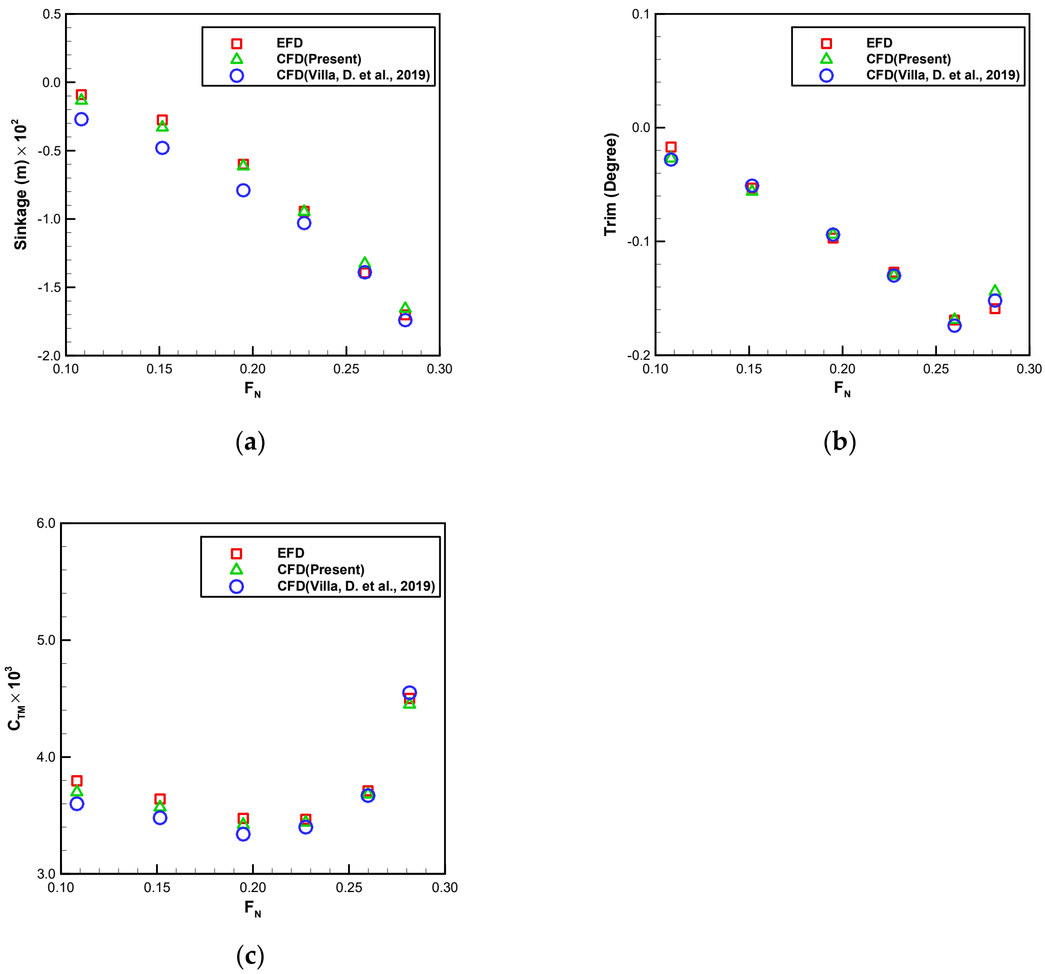

Figure 5. Comparison of KCS simulation results between EFD (Experimental Fluid Dynamics) and computational fluid dynamics (CFD) (a positive trim value was defined bow up and positive sinkage value was defined upward). (**a**) Sinkage; (**b**) trim; and (**c**) total resistance coefficient.

4.2. 8000 TEU-Class Container Ship

Numerical simulations were conducted under five different speed conditions (Froude number (F_N) 0.165, 0.192, 0.219, 0.247, and 0.274) for validation of the simulation conditions in a model scale. The results are as shown in Table 4 and Figure 6.

Similar to the KCS hull form, the sinkage tended to increase as the speed increased, and trim by head tended to increase as speed increased, when F_N was 0.247 or below and decreased when F_N was above 0.247. Sinkage was observed at a significant level in all cases where the superstructures were absent, and varied by approximately 3% to 9% between cases with superstructures. However, even as the speed increased, the quantitative difference remained consistent at approximately 0.0004. Trim was observed at a significant level at F_N of 0.2 or below when the superstructures were considered and at F_N of 0.2 or above when the superstructures were not considered.

Table 4. Comparison of the simulation results with and without a superstructure (RD—relative difference).

F_N	Sinkage (m) × 10^2			Trim (Degree)		
	With Superstructure	Without Superstructure	RD (%)	With Superstructure	Without Superstructure	RD (%)
0.165	−0.393	−0.433	9.2	−0.035	−0.032	−9.4
0.192	−0.558	−0.597	6.5	−0.055	−0.050	−10.0
0.219	−0.763	−0.807	5.5	−0.067	−0.069	2.9
0.247	−1.030	−1.070	3.7	−0.078	−0.082	4.9
0.274	−1.350	−1.400	3.6	−0.062	−0.065	4.6

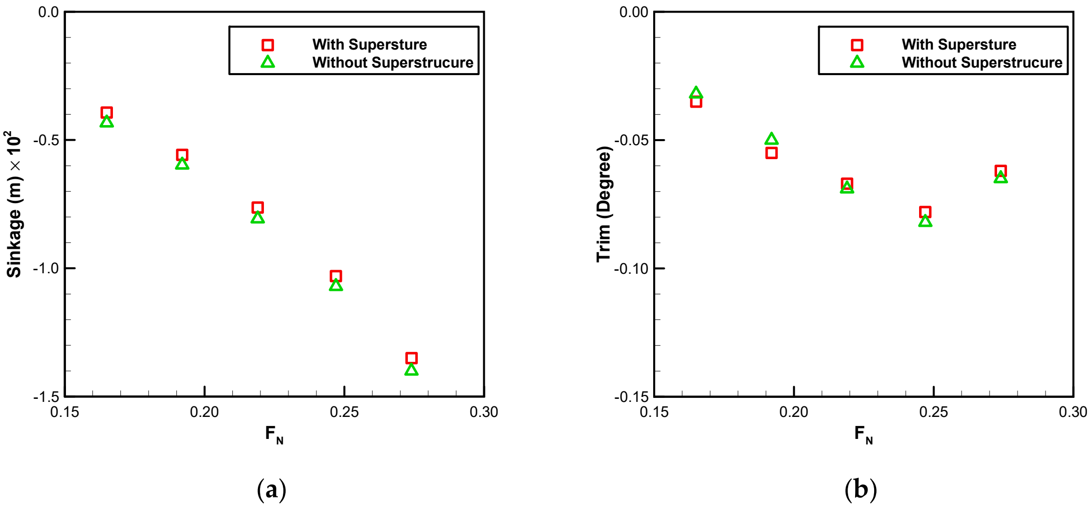

Figure 6. Comparison of simulation results with and without superstructures (a positive trim value was defined bow up and positive sinkage value was defined upwards). (**a**) Sinkage and (**b**) trim.

Wave patterns tended to become similar as the speed increased, with the biggest difference observed at the lowest speed (F_N 0.165) in Figure 7. Here, the vector distribution around the ship according to the presence or absence of the superstructure is shown in Figure 8.

C_{TM} differed by a maximum of approximately 2%, under five different speed conditions, with and without the superstructures, as shown in Figure 9a. When F_N was 0.2 or less, the resistance was higher in the case without superstructure and when F_N was 0.2 or above it showed opposite results. This showed a typical tendency where the trim by head had a relatively lower resistance, compared to the even conditions, or the trim by stern [15,16].

To analyze the effects of the presence or absence of superstructures on the resistance, the resistance performance of the full-scale ship was estimated using Equations (1)–(5). Here, C_{AA} obtained from Equation (5) was calculated using the coefficient in Table 5, for the case without the superstructure and C_{AA} was set to 0, when the superstructure was considered.

Table 6 and Figure 9b show that depending on whether C_{AA} is considered or not, C_{TS} differs by approximately 1% to 5%, under the six speed conditions and the difference was significant at approximately 5% when F_N was relatively low at 0.192 or below.

This indicated that calculation using an empirical formula could lead to over-estimation of the resistance performance of a full-scale ship, compared to a direct numerical interpretation, when considering the superstructures.

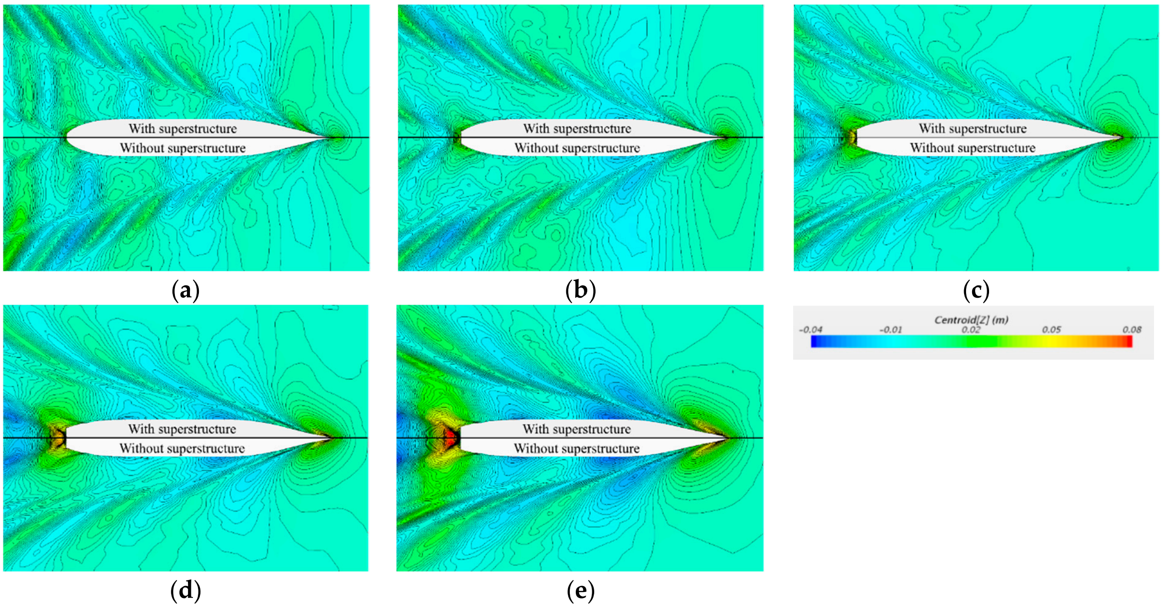

Figure 7. Comparison of wave pattern between the 8000 TEU container ship with superstructure and without superstructure. (**a**) F_N 0.165, (**b**) F_N 0.192, (**c**) F_N 0.219, (**d**) F_N 0.247, and (**e**) F_N 0.274.

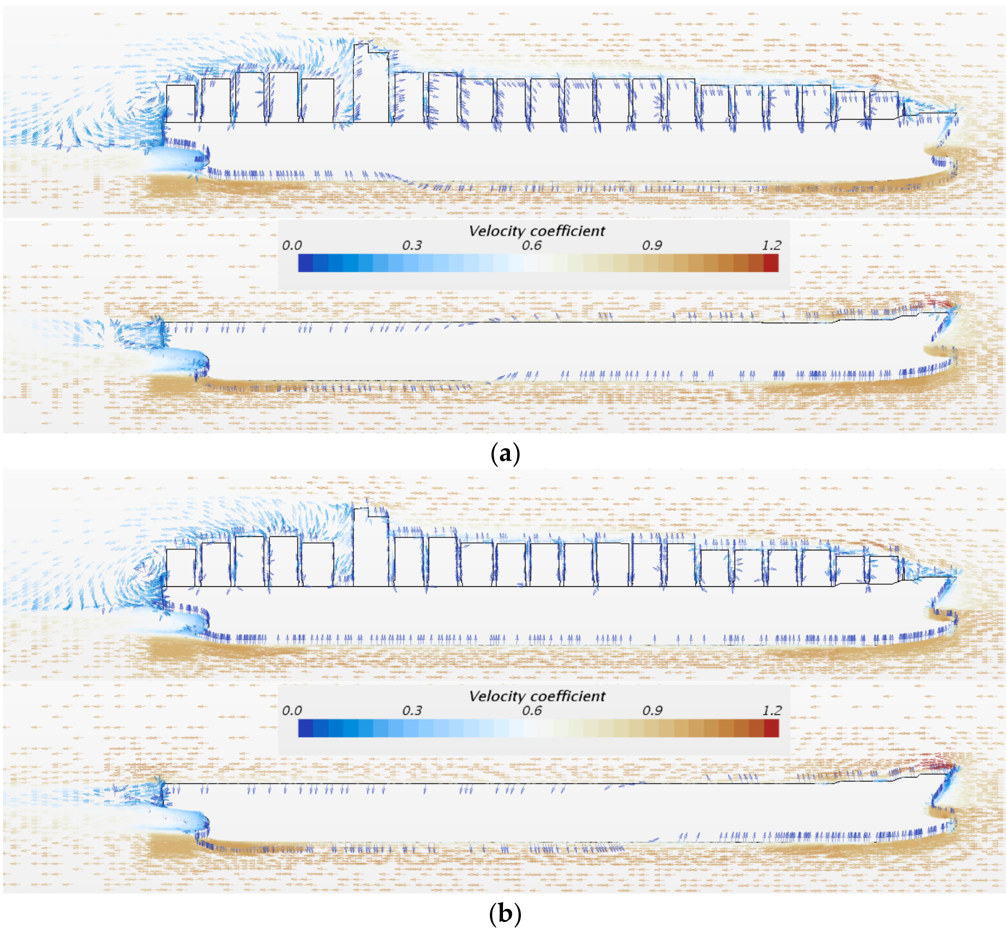

Figure 8. Velocity vector around the 8000 TEU-class container ship (velocity coefficient was defined as velocity divided by the inlet velocity). (**a**) F_N 0.165 and (**b**) F_N 0.274.

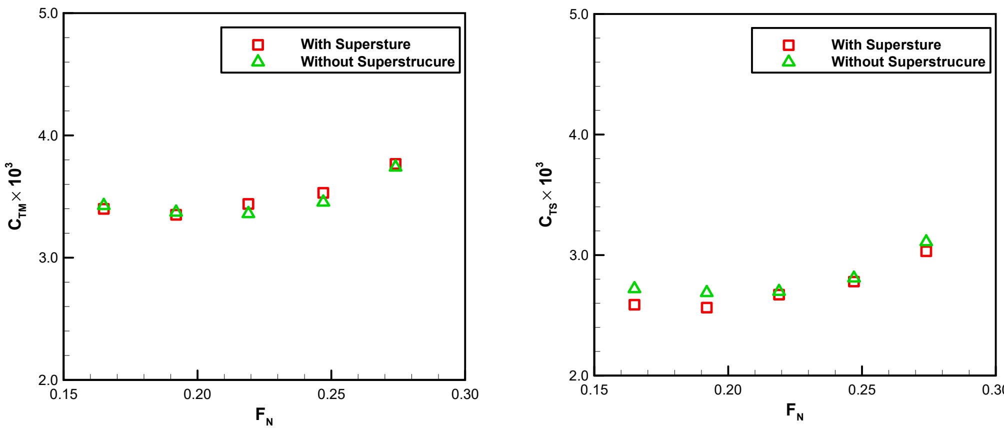

(**a**) (**b**)

Figure 9. Comparison of total resistance coefficient for ships, with and without a superstructure. (**a**) Model scale and (**b**) full scale.

To analyze the effects of overestimating the C_{AA}, the default value of C_{DA} by ITTC was compared with the C_{AA} for a container ship, calculated by Kristensen and Lützen [17] and the result of the equations proposed by Fujiwara et al. [18].

The C_{AA} proposed by Kristensen and Lützen [17] estimates the air resistance coefficient according to the loading capacity of a container ship, as shown in Equation (10), and is not more than 0.09.

$$C_{AA} \cdot 1000 = 0.28 \cdot TEU^{-0.126} \text{ less than } 0.09 \quad (10)$$

Table 5. Factors for calculating the air resistance coefficient.

C_{DA}	ρ_A	ρ_S	A_{VS}	S_S
0.8	1.23 kg/m^3	1025.9 kg/m^3	1742.1 m^2	16644.0 m^2

Table 6. Comparison of resistance coefficients with and without superstructure.

F_N	Condition	$C_{TM} \times 10^3$	$C_{FM} \times 10^3$	$C_R \times 10^3$	$C_{FS} \times 10^3$	$C_A \times 10^3$	$C_{AA} \times 10^3$	$C_{TS} \times 10^3$
0.165	With superstructure	3.403	2.153	1.249	1.369		-	2.593
	Without superstructure	3.430		1.276			0.1	2.720
	RD (%)	0.8	-	2.1	-		-	4.7
0.192	With superstructure	3.355	2.105	1.250	1.345		-	2.568
	Without superstructure	3.375		1.269			0.1	2.688
	RD (%)	0.6	-	1.5	-		-	4.5
0.219	With superstructure	3.443	2.065	1.377	1.324		-	2.676
	Without superstructure	3.363		1.298		−0.026	0.1	2.697
	RD (%)	−2.4	-	−6.1	-		-	0.8
0.247	With superstructure	3.534	2.030	1.504	1.307		-	2.784
	Without superstructure	3.457		1.427			0.1	2.808
	RD (%)	−2.2	-	−5.4	-		-	0.9
0.274	With superstructure	3.771	2.000	1.771	1.291		-	3.036
	Without superstructure	3.744		1.743			0.1	3.109
	RD (%)	−0.7	-	−1.6	-		-	2.3

The Fujiwara formula [18], which is mainly used for resistance correction in sea trials, is shown in Equations (11)–(14). The value of each parameter used in the calculation is provided in Table 7; Table 8. Figure 10 shows the profile of the 8000 TEU-class container ship used to calculate the coefficient values.

$$C_{DA} = C_{LF}\cos\varphi_{WR} + C_{XLI}\left(\sin\varphi_{WR} - \frac{1}{2}\sin\varphi_{WR}\cos^2\varphi_{WR}\right)\sin\varphi_{WR}\cos\varphi_{WR} + C_{ALF}\sin\varphi_{WR}\cos^3\varphi_{WR} \tag{11}$$

$$C_{LF} = \beta_{10} + \beta_{11}\frac{A_{YV}}{L_{OA}B} + \beta_{12}\frac{C_{MC}}{L_{OA}} \tag{12}$$

$$C_{XLI} = \delta_{10} + \delta_{11}\frac{A_{YV}}{L_{OA}h_{BR}} + \delta_{12}\frac{A_{XV}}{Bh_{BR}} \tag{13}$$

$$C_{ALF} = \varepsilon_{10} + \varepsilon_{11}\frac{A_{OD}}{A_{YV}} + \varepsilon_{12}\frac{B}{L_{OA}} \tag{14}$$

Here, A_{OD} is the lateral projected area of the superstructures, A_{XV} is the area of the maximum transverse section exposed to the wind, A_{YV} is the projected lateral area above the waterline, B is the ship breadth, L_{OA} is the overall length, C_{MC} is the horizontal distance from the mid-ship section to the center of the lateral projected area, h_{BR} is the height of the top of the superstructure, and φ_{WR} is the relative wind direction (0 indicates the wind heading). The values of the non-dimensional parameters (β_{ij}, δ_{ij}, ε_{ij}) are listed in Table 8.

The calculation results of C_{DA} are as shown in Table 9. Here, C_{AA} was calculated using the method proposed by Kristensen and Lützen [17], which is shown in Equation (10). The ITTC value was the counter-calculated value of C_{DA}, using Equation (5). The value of 0.67 calculated by the Fujiwara formula was the same result as the C_{DA} value of the 6800 TEU-class container ship, with containers in the laden condition, provided by ITTC [19]. The result indicated that ships with typical forms, such as a container ship, would show similar results.

The C_{DA} value was 16% lesser with the Fujiwara formula and 10% lesser with the method proposed by Kristensen and Lützen [17] than the ITTC value of 0.8, which was the default value of C_{DA}.

The results of estimating the total resistance coefficient by applying the C_{DA} calculated by the respective methods are shown in Table 10 and Figure 11. All three methods over-estimated the resistance values when compared with the numerical simulations in the case where the superstructures were considered, but the quantitative differences were reduced by using a C_{DA} value lower than the default value. For the Fujiwara formula, which used the lowest C_{DA} value, the difference was approximately at a 4%lower speed of F_N at 0.192 or below, but decreased to 2% or below at higher F_N.

Table 7. Parameters for calculating the Fujiwara formula.

A_{OD}	A_{XV}	A_{YV}	L_{OA}	B	C_{MC}	h_{BR}	φ_{WR}
4774.0 m^2	1742.1 m^2	8806.1 m^2	339.4 m	45.6 m	−10.8 m	45.0 m	0°

Table 8. Non-dimensional parameters for calculating the Fujiwara formula.

Parameter	i	j		
		0	1	2
β_{ij}	1	0.922	−0.507	−1.162
	2	−0.018	5.091	−10.367
δ_{ij}	1	−0.458	−3.245	2.313
	2	1.901	−12.727	−24.407
ε_{ij}	1	0.585	0.906	−3.239
	2	0.314	1.117	-

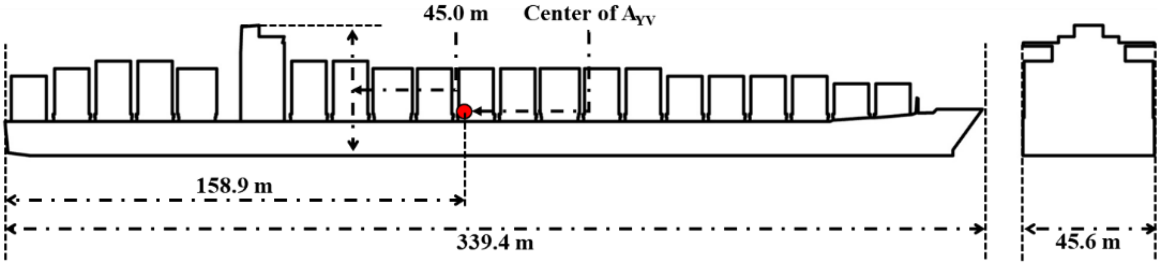

Figure 10. Schematic profile above the waterline for calculating the Fujiwara formula.

Table 9. Comparison of C_{DA} through different calculating methods.

Coefficient	ITTC (Default)	Fujiwara Formula	Kristensen and Lützen (2013)
C_{DA}	0.8	0.67	0.72
$C_{AA} \times 10^3$	0.100	0.084	0.090

Table 10. The total resistance coefficient according to C_{DA}.

F_N	$C_{TS} \times 10^3$			
	With Superstructure	Without Superstructure	Fujiwara Formula	Kristensen and Lützen (2013)
0.165	2.593	2.720	2.704	2.710
0.192	2.568	2.688	2.672	2.678
0.219	2.676	2.697	2.681	2.686
0.247	2.784	2.808	2.792	2.797
0.274	3.036	3.109	3.092	3.098

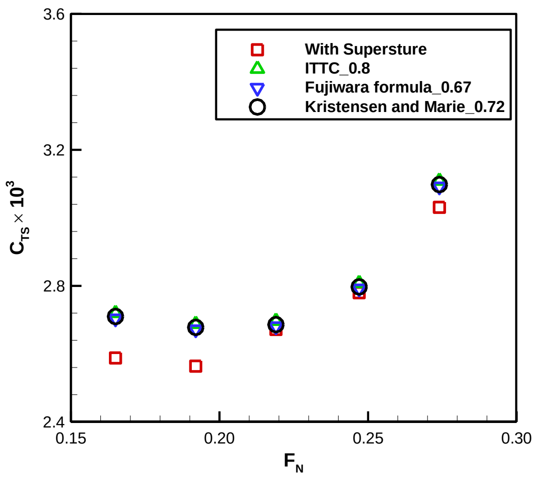

Figure 11. Comparison of total resistance coefficient by C_{DA}.

5. Conclusions

In this study, a numerical simulation was conducted on the 8000 TEU-class container ship to study the variation in resistance performance, according to the presence or absence of superstructures on a ship. Prior to the numerical simulation for the 8000 TEU-class container ship, numerical simulations using the KCS hull form were conducted to verify the numerical simulation conditions. The numerical simulation results of the KCS hull form for total resistance acting on the ship, showed a similar tendency as that observed for the experimental results, with a quantitative difference of approximately less than 3%. However, in the case of trim and sinkage, as excessive quantitative differences were observed at low and high speeds, numerical simulations for the 8000 TEU-class container ship was conducted at the F_N range of 0.16–0.27. The results of the study are summarized below:

- Trim

Trim tended to increase in volume as the speed increased at F_N of 0.247 or below and decreased at F_N above 0.247. Trim was significant with superstructures when F_N was 0.2 or below and without superstructures when F_N was 0.2 or above.

- Sinkage

Sinkage tended to increase as the speed increased. In the absence of superstructures, sinkage was significant with a difference of approximately 3% to 9% in the cases with superstructures. However, even as the speed increased, the quantitative difference remained consistent at approximately 0.0004.

- Total resistance coefficient

Under the five speed conditions, C_{TM} differed by a maximum of approximately 2% between ships, with and without superstructures. Here, when F_N was 0.2 or less, the resistance was higher in the case without superstructure and when F_N was 0.2 or above it showed the opposite results.

C_{TS} differed by approximately 1% to 5%, under the six speed conditions. The difference increased to approximately 5%, when F_N was at a relatively low speed of 0.192 or below. Overall, using an empirical formula overestimated the resistance performance of a full-scale ship in comparison to direct numerical analysis, when considering superstructures.

- Air resistance

To identify the effects of C_{DA}, C_{AA} was calculated using the method proposed by Kristensen and Lützen [17] and the Fujiwara formula [18]. The total resistance of the full-scale ship was estimated by incorporating the above result.

Both methods showed similar results as those of the numerical simulations that considered superstructures, when compared with the results obtained with C_{DA} of 0.8, which was the ITTC-proposed default value. However, a difference of approximately 4% was observed at the low speed of F_N = 0.192 or below. It is believed that the resistance performance of a full-scale ship could be more accurately estimated by calculating and using the C_{DA} obtained through wind tunnel testing, empirical formulas, and numerical analysis, rather than using the default value suggested by ITTC.

In addition, significant differences observed at low speeds were considered to be caused by the use of identical C_{AA} at all speeds. This is because C_{DA} was calculated in the high-speed range where the effects of the Reynolds number was absent through the Reynolds effect test, in the wind tunnel test or numerical simulation. Therefore, it might have led to errors in estimating the resistance performance of the ship at low speeds.

As mentioned above, it showed the difference in resistance performance between empirical methods and CFD with superstructure. This is because it was calculated only for the wind resistance, using the area of the superstructure and the wind load coefficient in the empirical methods. Thus, it did not consider the increase in resistance due to a change in the attitude of the ship in the empirical methods. Therefore, it was thought that a numerical simulation including superstructure for increasing accuracy about estimation of resistance performance should be performed. Especially, it was expected to be more useful for ships such as automobile ferries and LNG carriers, with a constant superstructure under ballast conditions. However, it was deemed necessary to conduct further studies on the methods of calculating air resistance, in relation to the presence or absence of superstructures and on various types of ships with large superstructures, in order to accurately estimate the resistance performance of a full-scale ship.

Author Contributions: J.S.; writing—original draft preparation; J.-C.P.; writing—review and editing. All authors have read and agreed to the published version of the manuscript.

Funding: This work was supported by the Technology Innovation Program (20000721, Development of Autopilot applicated collision avoidance technology for medium and large vessel) funded by the Ministry of Trade, Industry & Energy (MOTIE, Korea).

Conflicts of Interest: The authors declare no conflict of interest

References

1. Tezdogan, T.; Demirel, Y.K.; Kellett, P.; Khorasanchi, M.; Incecik, A.; Turan, O. Full-scale unsteady RANS CFD simulations of ship behaviour and performance in head seas due to slow steaming. *Ocean Eng.* **2015**, *97*, 186–206. [CrossRef]
2. Tezdogan, T.; Incecik, A.; Turan, O. Full-scale unsteady RANS simulations of vertical ship motions in shallow water. *Ocean Eng.* **2016**, *123*, 131–145. [CrossRef]
3. Wang, C.; Sun, S.; Li, L.; Ye, L. Numerical prediction analysis of propeller bearing force for full-scale hull–propeller–rudder system. *Int. J. Naval Archit. Ocean Eng.* **2016**, *8*, 589–601. [CrossRef]
4. Demirel, Y.K.; Turan, O.; Incecik, A. Predicting the effect of biofouling on ship resistance using CFD. *App. Ocean Res.* **2017**, *62*, 100–118. [CrossRef]
5. Song, S.; Demirel, Y.K.; Atlar, M. An investigation into the effect of biofouling on the ship hydrodynamic characteristics using CFD. *Ocean Eng.* **2019**, *175*, 122–137. [CrossRef]
6. ITTC. ITTC. ITTC Recommended Procedures and Guidelines. In *1978 ITTC Performance Prediction Method*; ITTC: Zurich, Switzerland, 2017.
7. Islam, H.; Soares, G. Effect of trim on container ship resistance at different ship speeds and drafts. *Ocean Eng.* **2019**, *183*, 106–115. [CrossRef]
8. Seo, D.W.; Park, H.S.; Han, K.M. Analysis of resistance performance for various trim conditions on container ship using CFD. *J. Ocean Eng. Technol.* **2015**, *29*, 224–230. [CrossRef]
9. Sun, J.; Tu, H.; Chen, Y.; Xie, D.; Zhou, J. A study on trim optimization for a container ship based on effects due to resistance. *J. Ship Res.* **2016**, *60*, 30–47. [CrossRef]
10. CD-Adapco. *STAR-CCM+ User Guide, Version 9.02*; CD-Adapco: Melville, NY, USA, 2014.
11. Kim, W.J.; Van, S.H.; Kim, D.H. Measurement of flows around modern commercial ship models. *Exp. Fluids* **2001**, *31*, 567–578. [CrossRef]
12. Bakica, A.; Gatin, I.; Vukčević, V.; Jasak, H.; Vladimir, N. Accurate assessment of ship-propulsion characteristics using CFD. *Ocean Eng.* **2019**, *175*, 149–162. [CrossRef]
13. Park, D.W.; Lee, S.B. The sensitivity of ship resistance to wall-adjacent grids and near-wall treatments. *Int. J. Naval Archit. Ocean Eng.* **2018**, *10*, 683–691. [CrossRef]
14. Villa, D.; Gaggero, S.; Gaggero, T.; Tani, G.; Vernengo, G.; Viviani, M. An efficient and robust approach to predict ship self-propulsion coefficients. *Appl. Ocean Res.* **2019**, *92*, 101862. [CrossRef]
15. Park, D.W.; Lee, S.B.; Chung, S.S.; Seo, H.W.; Kwon, J.W. Effects of trim on resistance performance of a ship. *J. Soc. Naval Archit. Korea* **2013**, *50*, 88–94. [CrossRef]
16. Han, K.M.; Park, H.S.; Seo, D.W. Study on Resistance Component of Container Ship According to Trim Conditions. *J. Ocean Eng. Technol.* **2015**, *29*, 411–417. [CrossRef]
17. Kristensen, H.O.; Lützen, M. *Prediction of Resistance and Propulsion Power of Ships*; Project No. 2010-56; Emissionsbeslutningsstøttesystem Work Package 2, Report No. 04; Technical University of Denmark and University of Southern Denmark: Copenhagen, Denmark, 2013.
18. Fujiwara, T.; Ueno, M.; Ikeda, Y. A new estimation method of wind forces and moments acting on ships on the basis of physical component models. *J. Japan Soc. Naval Archit. Ocean Eng.* **2005**, *2*, 243–255. [CrossRef]
19. ITTC. *ITTC Recommended Procedures and Guidelines: Preparation, Conduct and Analysis of Speed/Power Trials*; ITTC: Zurich, Switzerland, 2017.